Available online at www.sciencedirect.com
SCIENCE DIRECT®
International Journal of Mass Spectrometry 239 (2004) 77–86
International Journal of Mass Spectrometry
www.elsevier.com/locate/ijms

Atmospheric variability of biogenic VOCs in the surface layer measured by proton-transfer-reaction mass spectrometry

Thomas Karl*, Alex Guenther

National Center for Atmospheric Research, Boulder, CO, USA

Received 29 August 2003; accepted 14 September 2004
Available online 11 November 2004

Abstract

Fast response measurements of biogenic volatile organic compounds (VOC) using proton-transfer-reaction mass spectrometry (PTR-MS) were conducted above a deciduous temperate, a tropical rain and an evergreen needle forest. We explore how the variance of a compound relates to the surface flux and lifetime (τ) at these sites. Our results suggest that a modified variance method can be used for estimating surface fluxes of isoprene and methanol above sites characterized by homogenous surface emissions. The normalized variability σ_C/C, generally used for variability–lifetime relationships, increases as a function of averaging period, and follows an inverse lifetime-dependence. The variability of short-lived compound lies within the predicted range for mixed layer parameterizations such as the top-down (TD)–bottom-up (BU) variance functions. For lifetimes >1 day, significant deviation due to mesoscale processes adds to the variability on timescales above ~30 min.

Keywords: Atmospheric variability; Biogenic VOCs; Proton-transfer-reaction mass spectrometry; Homogeneous surface emissions

1. Introduction

Junge [1] introduced an empirical relation suggesting that the normalized variability σ_C/C (where C is the mean concentration and σ_C, the standard deviation) of a relatively long-lived atmospheric constituent ($\tau > 1$ year) should be inversely proportional to the lifetime, τ:

$$\sigma_C/C = 0.14\tau^{-1} \tag{1}$$

Subsequent studies based the original concept on modeling the source and sink terms as stochastic variables [2]. More recently, Ehhalt et al. [3] and Jobson et al. [4] have extended variability–lifetime relationships (VLRs) and showed that they can potentially be used for estimating lifetimes and trends of short-lived volatile organic compounds (VOCs). They argued that σ_C/C is proportional to τ^{-b} with b close to 0.5 far away from sources and approaching 0 the closer the receptor site is to the source region.

Lenschow and Gurarie [5] and Jaenicke [6] have shown that assuming a first-order decay (where c stands for the concentration of a species) with negligible contribution by transport,

$$\frac{\partial c}{\partial t} + \frac{c}{\tau} = 0 \tag{2}$$

the normalized variance can be expressed as

$$\left(\frac{\sigma_C}{C}\right)^2 = \frac{S}{2\tau}\coth\left(\frac{S}{2\tau}\right) - 1 \tag{3}$$

In the limit where the sampling time S is much shorter than the lifetime τ ($S \ll \tau$), (3) reduces to

$$\frac{\sigma_C}{C} \approx \frac{S}{2\sqrt{3}}\tau^{-1} \tag{4}$$

The coefficient $A = S/(2\sqrt{3})$ corresponds to Junge's original estimate of 0.14 years if the sampling time S is approximately 0.48 years. For the opposite case ($S \gg \tau$), (3) simpli-

* Corresponding author. Tel.: +1 303 497 1884; fax: +1 303 497 1477.
E-mail address: tomkarl@ucar.edu (T. Karl).

1387-3806/$ – see front matter © 2004 Elsevier B.V. All rights reserved.
doi:10.1016/j.ijms.2004.09.023

fies to

$$\frac{\sigma_C}{C} \approx \sqrt{\frac{S}{2}}\tau^{-1/2} \quad (5)$$

This simple example illustrates how the variability trend depends on the sampling interval (S) and lifetime (τ). It is interesting to note that more detailed 2D and 3D models [3] produced a similar lifetime-dependence (with $b \cong 1/2$) for continental sources of various species.

Lenschow and Gurarie [5] described a 1D vertical diffusion model for relating fluctuations of homogenously distributed scalars to their lifetimes in the atmosphere. They showed that the variability in the free troposphere can be related to mixing processes between the planetary boundary layer (PBL), the free troposphere (FT) and the stratosphere (S). On the other hand, Wyngaard and Brost [7] proposed that scalar transport in the convective PBL, which is typically well mixed, can be described in terms of the superposition of top-down (TD) and bottom-up (BU) processes. Using large-eddy simulations (LES), they inferred TD–BU flux-gradient and -variance relationships for the PBL. The variance functions (σ_C) are parameterized using convective scaling as follows:

$$\sigma_C^2 = \left(\frac{F_e}{w^*}\right)^2 f_t(z/z_i) + \left(\frac{F_s}{w^*}\right)^2 f_b(z/z_i) + 2\left(\frac{F_e F_s}{w^{*2}}\right) f_{tb}(z/z_i) \quad (6a)$$

$$f_t\left(\frac{z}{z_i}\right) \cong 3.1\left(1 - \left(\frac{z}{z_i}\right)\right)^{-2/3} \quad (6b)$$

$$f_b(z/z_i) \cong (z/z_i)^{-0.9} \quad (6c)$$

$$f_{tb}(z/z_i) = 0.5(f_t f_b)^{1/2} \quad (6d)$$

where F_e is the entrainment flux; F_s, the surface flux; w^*, the convective velocity scale; z, the height above ground and z_i, the boundary layer height. The convective velocity scale is commonly calculated from the sensible heat flux ($\overline{w'T'}$), temperature (T), gravitational constant (g) and the boundary layer height (z_i):

$$w^* \equiv \left(\frac{g}{T}\overline{w'T'}z_i\right)^{1/3} \quad (7)$$

Originally, the TD–BU functions were derived from simulations that did not include the influence of a forest canopy explicitly. Patton et al. [8] presented modified gradient TD–BU functions due to the influence of a canopy, which is known to increase the mixing efficiency in the roughness sub layer. Their results showed that the bottom-up function (f_b) was mainly affected. They suggested using,

$$f_b(z/z_i) = 1.5((z-d)/z_i)^{-3/5}, \quad (8)$$

for canopies with a leaf area index (LAI) of ~2, where d is the displacement height.

A number of studies using proton-transfer-reaction mass spectrometry (PTR-MS) have recently demonstrated the usefulness of VLRs in estimating sink terms and trends of VOCs in remote locations far away from emission sources [9–12]. We extend these efforts by investigating the applicability of variability measurements in the surface layer (SL) above a homogenously distributed source region. A set of biogenically emitted trace species (isoprene, methanol and acetone) is used to test variability predictions inferred from the TD–BU approach [6] as well as a 1D vertical diffusion model [5] at two locations (a deciduous hardwood forest in Northern Michigan and a tropical rainforest in Costa Rica). In addition, we show how the variance of VOCs can be related to the surface flux taking datasets from three experiments (Prophet tower, Michigan, CARBONO tower, Costa Rica, and FACTS-I tower at Duke Forest, North Carolina). The variance method could provide an alternative to eddy covariance and disjunct eddy covariance measurements, which have been previously successfully deployed for estimating surface emissions using the PTR-MS [13–15]. We demonstrate that the ability to perform fast response measurements of VOCs is particularly advantageous when investigating turbulent exchange processes in the atmosphere.

2. Results

The PTR-MS system was recently deployed for biogenic VOC emission measurements at the Prophet tower (45.55N, 84.71W) of the UMBS (University of Michigan Biological Station)), situated in the transition zone between the mixed hardwood and boreal forests in Northern Michigan (2002), at the La Selva Biological Station (10.43N, 83.93W) in the lowland tropical wet forests in the canton Sarapiqui, province of Heredia, Costa Rica (2003) and at a loblolly pine plantation at the Duke FACTS-1 site (forest–atmosphere carbon transfer and storage) (35.98N, 79.09W) in North Carolina (2003). Sampling setup and measurement protocols for flux measurements were previously described in detail [14,15]. In addition, the reader is referred to the following papers [16–18] for a detailed description of the operation/performance of the PTR-MS instrument.

We chose to investigate the variability of the dominant biogenic VOCs on 3 days at each site between 08:00 and 16:00 local time, which were characterized by fair weather conditions with little or no clouds and no precipitation. The dominant biogenic hydrocarbon at both sites was isoprene, followed by methanol. In addition to these two compounds, acetone was consistently emitted, with a seasonal variation observed at the hardwood forest in Michigan. Other oxygenated VOCs such as acetaldehyde, acetic acid + glycolaldehyde and MVK + MAC showed more complex surface exchange patterns due to the fact that they are partially (acetaldehyde) or exclusively (MAC + MVK) produced by photochemical reactions on relatively short timescales. These compounds showed both emission and deposition fluxes especially in

the tropics and were, therefore, excluded from the current analysis, which primarily attempts to investigate the relationship between emission fluxes and the normalized variability (σ_C/C).

We used wavelet analysis for analyzing the localized variations of power within individual time series [19]. The main advantage of wavelet analysis lies in determining both the dominant modes of variability (such as with conventional Fourier transformation) and the time dependence of those modes. In addition, the variability can be integrated over certain periods and wavelengths (frequencies) to obtain scale-averaged and/or time averaged variances. As an example, Fig. 1 shows the wavelet decomposition of isoprene using the Morlet wavelet as basis function [19,20]. The top panel depicts the diurnal variation of the isoprene concentration observed on 9th June 2002 at the Prophet tower in Michigan. The variance contained in this signal is broken up into a frequency–time space as shown in the middle left panel. In the particular case, the wavelet transformation was constructed using eight octaves (32 s (0.03 Hz) to 4096 s (0.00024 Hz)) over the 14.7 h ($\sim 53 \times 10^3$ s) sampling period. Short-term variations of the isoprene concentration for example are evident at approximately 5–7 h (18×10^3 to 25×10^3 s) after the measurement was started, causing an increased variability on a timescale of >1.1 h ($\sim$4096 s). This mode was caused by a shift in air masses in conjunction with clouds and the associated variations affecting ambient isoprene concentrations. Shorter features on scales <20 min (<1024 s) are mostly related to convective turnaround times in the boundary layer. The righthand side in Fig. 1c shows the global wavelet spectrum, defined as the time averaged variance, which approaches a smoothed Fourier power spectrum over the same period. The spectral analysis of the VOC dataset cuts off at 24 (12) s in Michigan (Costa Rica), due to the disjunct sampling strategy used for the direct flux measurements [15]. In order to examine the variance over a wide range of scales (or bands), the scale-averaged wavelet power for five different bands (60–300, 60–600, 60–1800, 60–3600, 60–7200 s) were calculated. The lowest panel in Fig. 1 shows the differences between band 5 (60–7200 s), carrying the highest variability, and bands 1–4 having shorter band-widths. The range of the observed absolute values for each band during midday conditions was subsequently used for the variability–lifetime plots in Fig. 2a and b. The variance resulting from instrumental noise and counting statistics was subtracted from these traces but had mainly an impact on the 60–300 and 60–600 s bands. For example, taking an average H_3O^+ primary ion density of 2.5×10^6 cps, a sensitivity of 37 cps/ppbv, an average ambient concentration of 3 ppbv, a dwell time of 0.2 s and a disjunct time gap of 11 s (one sample/11 s), the variability (σ_C/C) due to counting statistics was 39.2×10^{-3}, 27.7×10^{-3}, 16.0×10^{-3}, 11.3×10^{-3} and 8×10^{-3}, respectively, for the five bands (60–300, 60–600, 60–1800, 60–3600, 60–7200) investigated. Wider bandwidths averaged sufficiently long over the white noise contribution from the counting statistics. Fig. 2a and b depicts the normalized variability (σ_C/C) of isoprene, methanol and acetone for the five bands versus their estimated lifetimes τ for Costa Rica (La Selva) (Fig. 2a) and Michigan (Prophet) (Fig. 2b). Lifetimes for the La Selva experiment were based on estimated loss rates with respect to HO radicals using a photochemical box model [21], for Michigan lifetimes were based on HO measurements in 2001 [22]. In addition, predictions from a 1D diffusion model (gray solid and dash-dotted lines) were calculated for a 1 km (1.5 km) deep boundary layer at Prophet (La Selva) and a 15 km deep troposphere [5]. The normalized variability was related to the concentration difference between the boundary layer (C_{BL}) and the bottom of the free troposphere ($C_{FT}(z_B)$):

$$\frac{\sigma_C}{C} \equiv \frac{C_{BL} - C_{FT}(z_B)}{C_{BL}} \tag{9}$$

The difference between the two curves captures the range of vertical diffusivities (K_2) in the free troposphere, 1–10 $m^2\ s^{-1}$. More details about the model initialization can be found in Table 1 and [5]. Also plotted are results from the TD–BU parameterizations relating surface fluxes and entrainment fluxes to the observed variability in the BL using Eqs. (6)–(8) (shaded area) and the 1D-model output. The TD–BU parameterization should give a lower limit of the variability proportional to the surface emission [5]. It is noted that the modified f_b function (8) had a relatively small effect when compared to the change resulting from the different eddy diffusivities (K_2 = 1–10 $m^2\ s^{-1}$) in the FT. Below 0.12 days ($\sim$3 h), the TD–BU solution became unstable because the 1D vertical diffusion model could not be applied accurately [5]. The lighter shaded curves are extrapolated towards lower lifetimes based on the slopes at 0.12 days.

It appears that the normalized variability of isoprene lies within the range expected from the TD–BU functions. For methanol and acetone, which have lifetimes longer than 1 day, it is mainly the variability over small time scales (up to 600 s) that can be captured by the TD–BU functions. The larger scale variability cannot be represented since the TD–BU diffusion only incorporates turbulent processes on timescales related to PBL exchange. Since both methanol and acetone are expected to have higher background concentrations than short-lived compounds such as isoprene, mesoscale variability (e.g., in advected air masses) can add to the observed increase in variability seen for these compounds. It is noted that the normalization of the variance (σ_C/C) eliminates contributions of varying surface fluxes on timescales larger than the characteristic turbulence time scale $\sim 0.7 z_i/w^*$ [23], approximately $\sim$12 min for a boundary layer height of 1 km and a convective velocity scale w^* of 1 m/s. Acetone and methanol emissions are mainly temperature driven [24] typically varying over much longer timescales than this. The variability of all compounds gradually approaches the range predicted by the 1D diffusion model; that is, all of the 2-h values already lie close or between the lower and upper bounds calculated from the 1D diffusion model. This supports findings by Wang et al. [25] who reported that the normalized standard devia-

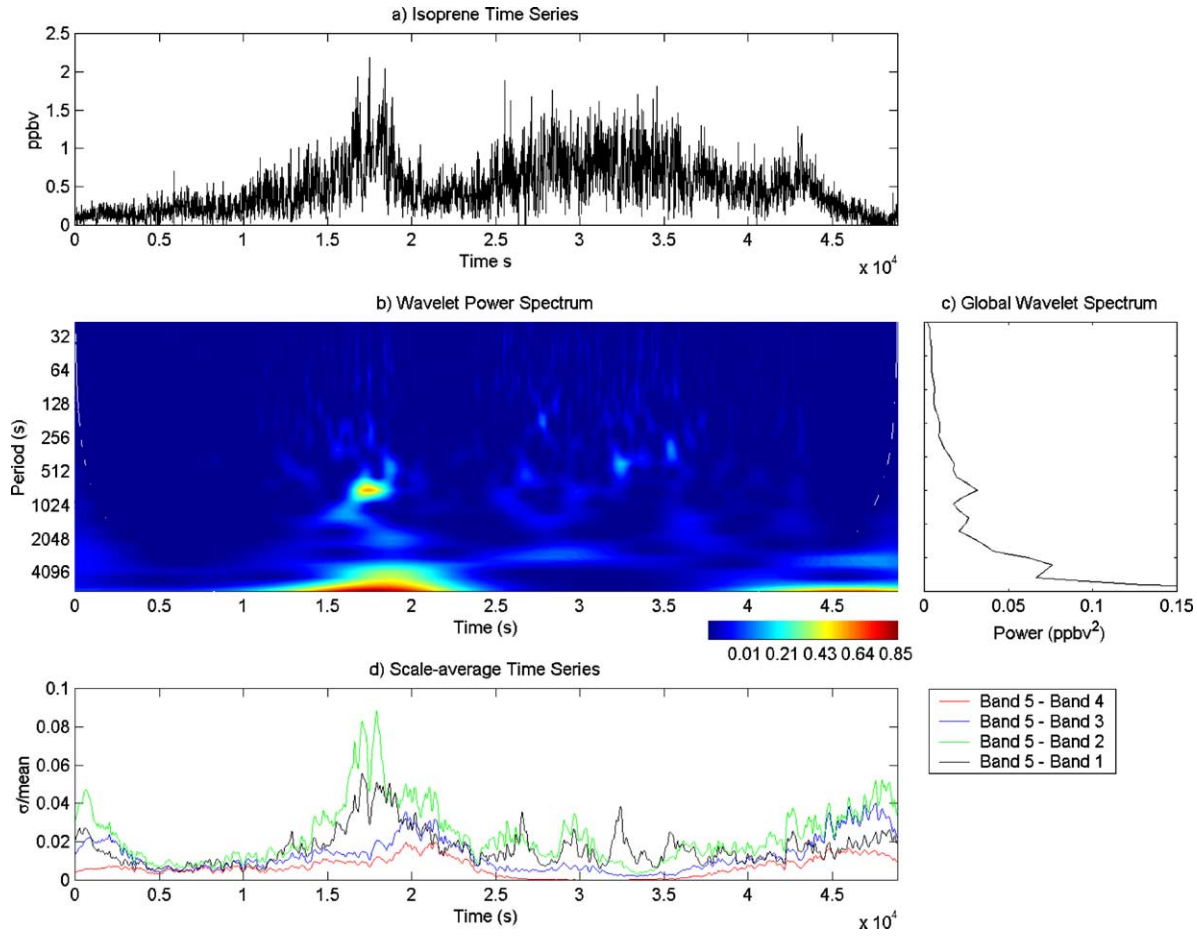

Fig. 1. Top panel (a): measured isoprene concentrations over the course of several hours. Middle left panel (b): wavelet decomposition of the isoprene signal using the Morlet wavelet and eight octaves (32 s (0.03 Hz)–4096 s (0.00024 Hz)) over the 14.7 h ($\sim 53 \times 10^3$ s) sampling period. Middle right panel (c): averaged global wavelet spectrum. Lower panel (d): the difference between the normalized variance (σ_C/C) of band 5 and bands 1–4, defined as: band 1, 60–300; band 2, 60–600; band 3, 60–1800; band 4, 60–3600; band 5, 60–7200.

Table 1
Parameters used for the 1D model calculation and the variance method

	z_i (m)	w^* (m/s)	K_2 (m^2/s)	z (m)	z/z_i	sqrt(f_b)
La Selva high	2000	1.2	10	40	0.020	5.5
La Selva low	500	2.10	1	40	0.080	3.6
Prophet high	1800	1.25	10	35	0.020	5.6
Prophet low	1000	2.20	1	35	0.035	4.7
Used in Table 2						
La Selva	1500	1.61	–	40	0.027	5.1
Duke	1500	1.50	–	30	0.020	5.5
Prophet	1500	1.72	–	35	0.023	5.3

tions of several photochemically reactive species emitted by the ocean during NASA PEM-Tropics-A were much larger than predicted by TD–BU diffusion and based on their estimated lifetimes for eddy sizes on the order of $\sim 5z_i$. These observations were collected in the Marine BL. Interestingly, we observe a very similar behavior for methanol and acetone in the SL above forested regions. This bias can arise from mesoscale variability such as cumulus convection, which can be important in the tropics, or Kelvin Helmholtz instabilities across the BL top, followed by horizontal advection and intermittent localized turbulence diffusion on much longer time scales than mixed layer turbulence [26]. In addition, non-homogenous surface emissions can also influence the variability. In the mixed layer (ML), the 'chewing up' of larger scale horizontal variations was recently described as a 'log-chipper' component in BL turbulence and investigated using LES [27]. The magnitude of this component could be on the order of the TD–BU variance functions and offset the calculated variability by 30% in the mixed layer (between $z/z_i = 0.3$ and 0.8), while playing a relatively small role in the SL (e.g.,

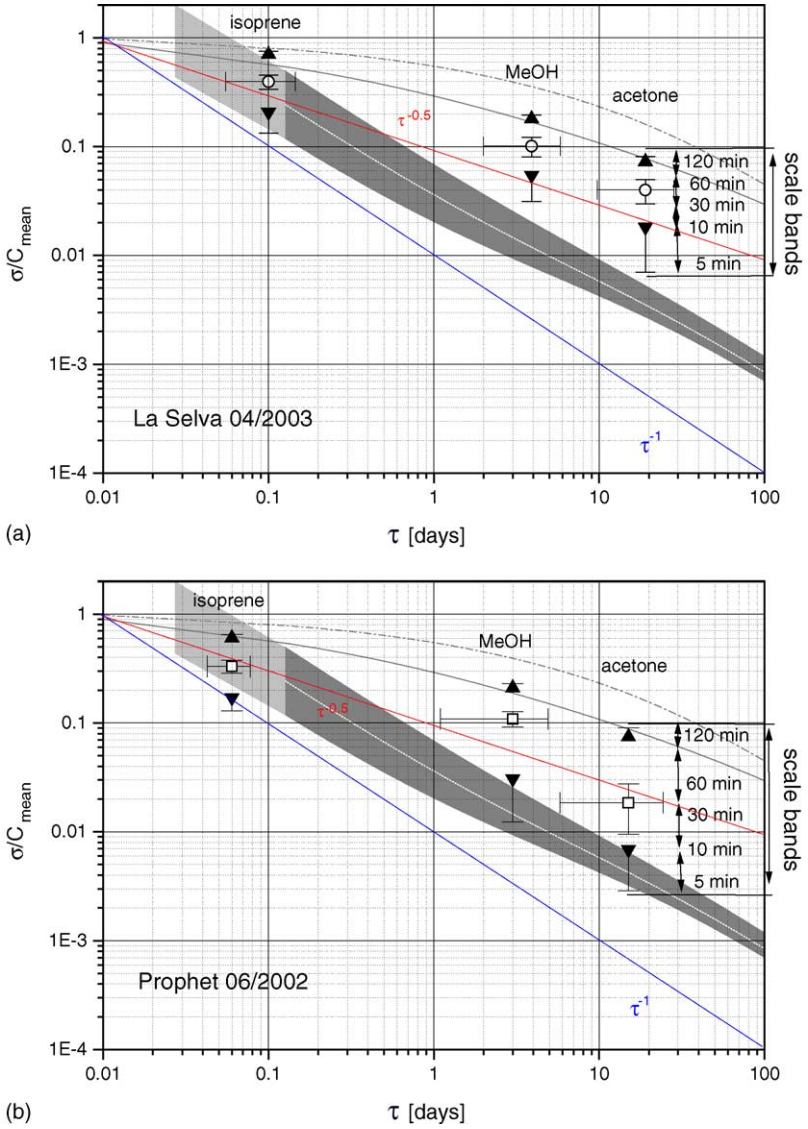

Fig. 2. (a) Variability lifetime plot of isoprene, methanol (MeOH) and acetone for the range of normalized variances (σ_C/C) calculated for three individual days and based on the five bands defined in Fig. 1 for La Selva. The distance between the lower whiskers and the lower down pointing solid triangles corresponds to the variability observed for bandwiths between 5 and 10 min (bands 1 and 2), open circles correspond to the mean variance for the 30 and 60 min bands (3 and 4) with lower and upper bounds represented by the Y-error bars. Horizontal error bars indicate the range of expected lifetimes. The upward pointing solid triangles correspond to variances observed for the 120 min bands (5) together with upper limits presented by the upper whiskers. The dark shaded curves were calculated from the TD–BU variance functions with upper and lower bounds based on the model output from the 1D Diffusion model and were extrapolated towards lower lifetimes (<0.1 days) indicated by the lighter shaded gray area. The gray solid ($K_2 = 1\,m^2\,s^{-1}$) and dash-dotted ($K_2 = 10\,m^2\,s^{-1}$) curves show the range of (σ_C/C) inferred from the 1D diffusion model. Also shown are lines depicting the τ^{-1} (blue) and $\tau^{-0.5}$ (red) dependence. (b) Same as 2a for data collected at Prophet (MI).

$z/z_i < 0.05$). Our observations suggest that a variability of up to 10 min lies within the range of the TD–BU predictions for the longer lived compounds, methanol and acetone.

How much of the surface flux is still captured at sampling rates >6 s (La Selva) and 12 s (Prophet)? The vertical flux is usually transported on temporal scales between 0.1 and 1800 s. Fig. 3 illustrates the peak intensities of the normalized heat flux spectra ($w'T'$) measured by a sonic anemometer for a ~2.8 h midday period (5×10^{-4} to 1×10^{-4} Hz) in Michigan. The spectral peak of the covariance between the vertical windspeed (w) and temperature (T) multiplied by the frequency typically occurred between 10 and 300 s (0.1–0.003 Hz) at all sites, characterizing canopy scale turbulence with characteristic horizontal eddies in canopy-scale flows ~8–9 times the canopy height h_c. [28]. These eddies are known to carry between 40% and 75% of the vertical flux. Using an average windspeed between 1 and 3 m/s and a canopy height of 30–40 m, the dominant eddy scale in the SL would be expected to be on the order of ~80–360 s. This suggests that a large portion of the variance attributed to the vertical flux was still contained in the timeseries measured at sampling rates on the order from 6 s (La Selva) to 12 s

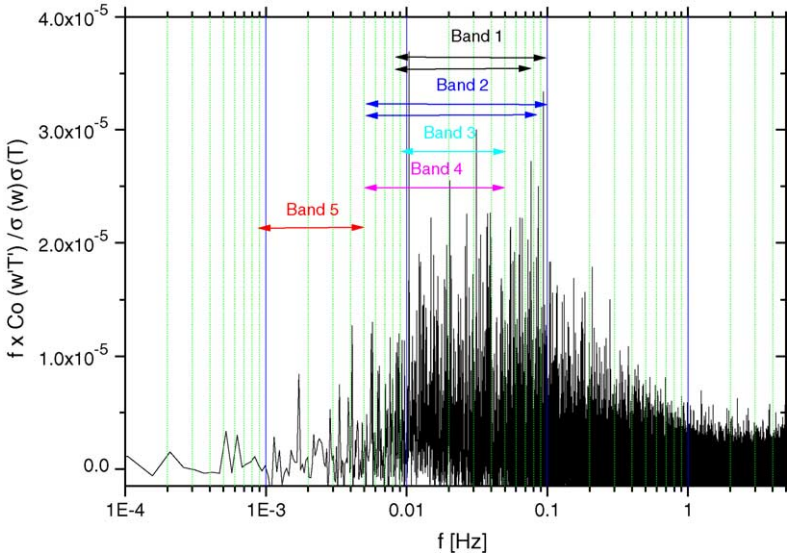

Fig. 3. The normalized cospectrum Co ($w'T'$) between the vertical wind speed (w) and temperature (T) multiplied by the frequency f and plotted vs. frequency f. The individual arrows indicate individual bandwidths for five bands that were subsequently used for the variance method.

(Prophet). It should, therefore, be possible to relate the VOC variability to the surface flux even if the sampling rate was on the order of roughly 10 s. As indicated in Fig. 3, five different bandwidths were chosen for the present analysis.

Assuming a typical entrainment velocity of 0.004 m s^{-1} [29], a concentration gradient between the PBL and the FT of 0.5 ppbv and a surface layer flux of 1 mg m^{-2} h^{-1}, the contributions of the f_t and f_{bt} terms in Eq. (6a) are small and on the order of 0.06% and 2.4%, respectively (at $z/z_i = 0.02$). Thus, under ideal conditions (homogenous surface emissions), the variance of a concentration measurement in the SL can be related to the surface flux through a simplified TD–BU variance equation:

$$\sigma_C^2 \approx \left(\frac{F_s}{w^*}\right)^2 f_b(z/z_i). \tag{10}$$

In theory, the variance over the whole temporal spectrum of eddies (e.g., 0.1–1800 s) would need to be taken into account. However, by introducing a proportionality constant (P_{scale}), one can relate the variance (σ_C) over a smaller period (range of eddy sizes) to the surface flux (F_s) according to:

$$\frac{(\sigma_C)_{scale}}{\sqrt{f_b(z/z_i)}} \approx P_{scale}\left(\frac{F_s}{w^*}\right), \tag{11}$$

The variance method is somewhat more susceptible to errors resulting from mesoscale processes than the eddy covariance method, where the cross correlation between the vertical wind speed and the concentration measurement prevents a large bias due to large scale variability. Thus, a better strategy is to apply the variance method over a relatively narrow time span. For example, the standard deviation over a 600 s interval of a 5 s averaged signal [in ppbv] can be related to the surface flux [in g m^{-2} s^{-1}] *via* the proportionality constant P_{scale} (5–600 s) and Eq. (12):

$$F_s \approx \frac{w^*(\sigma_C)_{scale}}{P_{scale}\sqrt{f_b(z/z_i)}}\frac{M_w \times 10^{-9}}{V_m}, \tag{12}$$

with M_w being the molecular weight and V_m the molar volume.

Alternatively, surface layer scaling variables are used more commonly [30] in the SL; similarly to Eq. (12), the surface flux (F_s) can be related to the friction velocity (u^*), measurement height (z), proportionality constant (F_{scale}) and the Monin-Obukhov length (L) [31]:

$$\begin{aligned} F_s &\approx \frac{u^*(\sigma_C)_{scale}}{F_{scale} f(z/L)}\frac{M_w \times 10^{-9}}{V_m} \\ f(z/L) &= (-(z-d)/L)^{-1/3} \quad \text{for}: z/L < -0.31 \end{aligned}, \tag{13}$$

Using the definitions from Eqs. (12) and (13), the proportionality constants (P_{scale} and F_{scale}) for five individual bands are summarized in Table 2 and were chosen as: band 1, s0–300 s; band 2: 60–300 s; band 3: s0–600 s; band 4: 60–600 s; band 5: 600–1800 s (with s0 being twice the sampling rate at Prophet (∼24 s) and La Selva (∼12 s)). The second column in Table 2 lists the observed range of surface fluxes (F_s) for which the proportionality constants (P_{scale}, F_{scale}) were calculated (typically between 10:00 and 15:00 local time). The white noise contribution from counting statistics was subtracted from the individual bands. Due to a relatively high background count rate (50–100 cps) for m/z 33$^+$, which corresponds to protonated methanol, the variances within bands 1 and 3 were dominated by white noise, and therefore, discarded. The total white noise level was based on the averaging time for each band and calculated as the starting time multiplied by the dwell time (integration time per m/z ratio) divided by the sample distance (due to disjunct sampling). For La Selva, for example, the total integration time for methanol for bands 2 and 4 yielded 5 s: 60 s (start-

Table 2
Proportionality constants P_{scale} and F_{scale} (columns 3–8), calculated for La Selva and Prophet

	Flux	P_{scale}	S0–300	60–300	S0–600	60–600	600–1800
Prophet (mg/m^{2}h)							
Isoprene	4.3 ± 1.2	Day1	0.48	0.59	0.61	0.52	0.35
	1.0 ± 0.5	Day2	0.40	0.35	0.43	0.40	0.32
	0.2 ± 0.01	Day3	0.49	0.76	0.54	0.86	0.79
		Average	0.46 ± 0.05	0.56 ± 0.21	0.53 ± 0.09	0.59 ± 0.24	0.49 ± 0.26
MeOH	1.2 ± 0.3	Day1	–	0.70	–	0.47	0.25
	1.3 ± 0.3	Day2	–	0.50	–	0.44	0.34
	0.5 ± 0.02	Day3	–	0.76	–	0.81	0.91
		Average	–	0.66 ± 0.13	–	0.57 ± 0.20	0.50 ± 0.36
La Selva							
Isoprene	1.5 ± 0.8	Day1	1.10	1.10	1.19	1.27	0.80
	1.7 ± 0.5	Day2	0.93	0.93	0.97	1.10	0.59
	1.7 ± 0.7	Day3	0.80	0.76	0.85	0.93	0.47
		Average	0.95 ± 0.15	0.93 ± 0.17	1.00 ± 0.17	1.10 ± 0.17	0.62 ± 0.17
MeOH	0.3 ± 02	Day1	–	1.27	–	1.35	0.72
	0.3 ± 0.1	Day2	–	0.93	–	1.02	0.42
	0.3 ± 0.1	Day3	–	0.89	–	0.97	0.42
		Average	–	1.03 ± 0.21	–	1.11 ± 0.21	0.52 ± 0.17
Duke							
Isoprene	0.7 ± 0.2	Day1	–	1.45	–	1.68	1.13
	0.7 ± 0.2	Day2	–	1.26	–	1.51	0.87
	0.8 ± 0.4	Day3	–	1.10	–	1.26	0.79
		Average	–	1.27 ± 0.18	–	1.48 ± 0.21	0.93 ± 0.18
MeOH	0.3 ± 0.1	Day1	–	3.16	–	3.46	1.79
	0.3 ± 0.1	Day2	–	2.96	–	3.21	1.26
	0.2 ± 0.1	Day3	–	2.69	–	2.89	1.20
		Average	–	2.93 ± 0.24	–	3.19 ± 0.29	1.42 ± 0.32
	Flux	F_{scale}	S0–300	60–300	S0–600	60–600	600–1800
Prophet							
Isoprene	4.3 ± 1.2	Day1	0.49	0.59	0.63	0.53	0.36
	1.0 ± 0.5	Day2	0.39	0.34	0.41	0.37	0.31
	0.2 ± 0.01	Day3	0.47	0.72	0.51	0.81	0.75
		Average	0.45 ± 0.05	0.55 ± 0.20	0.52 ± 0.11	0.57 ± 0.22	0.47 ± 0.24
MeOH	1.2 ± 0.3	Day1	–	0.71	–	0.48	0.25
	1.3 ± 0.3	Day2	–	0.48	–	0.42	0.32
	0.5 ± 0.02	Day3	–	0.72	–	0.76	0.86
		Average	–	0.64 ± 0.14	–	0.78 ± 0.26	0.30 ± 0.05
La Selva							
Isoprene	1.5 ± 0.8	Day1	1.21	1.21	1.33	1.41	0.89
	1.7 ± 0.5	Day2	1.33	1.33	1.37	1.53	0.85
	1.7 ± 0.7	Day3	0.77	0.73	0.81	0.89	0.44
		Average	1.10 ± 0.30	1.09 ± 0.32	1.17 ± 0.31	1.28 ± 0.34	0.73 ± 0.25
MeOH	0.3 ± 02	Day1	–	1.41	–	1.49	0.81
	0.3 ± 0.1	Day2	–	1.33	–	1.45	0.60
	0.3 ± 0.1	Day3	–	0.85	–	0.93	0.40
		Average	–	1.19 ± 0.30	–	1.29 ± 0.31	0.60 ± 0.20

Table 2 (*Continued*)

	Flux	P_{scale}	S0–300	60–300	S0–600	60–600	600–1800
Duke							
Isoprene	0.7 ± 0.2	Day1	–	1.10	–	1.27	0.86
	0.7 ± 0.2	Day2	–	0.96	–	1.15	0.66
	0.8 ± 0.4	Day3	–	0.83	–	0.96	0.60
		Average	–	0.96 ± 0.13	–	1.13 ± 0.16	0.71 ± 0.13
MeOH	0.3 ± 0.1	Day1	–	2.40	–	2.64	1.37
	0.3 ± 0.1	Day2	–	2.26	–	2.45	0.96
	0.2 ± 0.1	Day3	–	2.05	–	2.22	0.91
		Average	–	2.23 ± 0.18	–	2.44 ± 0.21	1.08 ± 0.25

Column 2 shows the observed range of fluxes on each day. S0 corresponds to 12 s at La Selva and 24 s at Prophet.

ing time of band 2) × 0.5 s (dwell)/6 s (sample distance). The sensitivity of the variance method for shorter bandwidths can be increased by using higher sampling rates (e.g., scanning over a smaller range of masses) or alternatively, by longer averaging times and bandwidths. However, the tradeoff for using longer bandwidths is that inhomogenous surface emissions can bias the observed variability. In the present case, 60 s averaging time (equal to a total integration time of 5 s) was sufficiently long for methanol. At the Prophet tower and the site in Costa Rica, all five bandwidths and averaging times were used for isoprene due to a sufficiently high flux, higher sensitivity and lower background. At all sites, no correlation for acetone was observed, which we attribute to a long lifetime and small surface flux. The Duke forest was the most heterogeneous site with isoprene originating mostly from the understory (sweetgum). Somewhat lower isoprene fluxes and higher instrumental background caused a rather poor correlation for bands 1 and 3, which were, therefore, discarded.

According to Eqs. (12) and (13), the P_{scale} and F_{scale} values represent the fraction of the total flux contained within each individual bandwidth. Assuming perfect homogeneous surface emissions these scaling factors should be smaller than 1 as they only cover a fraction of the whole eddy spectrum transporting the vertical flux (the flux measurements were calculated for 30 min periods). For a band covering all timescales between 0.1 and 1800 s, the total scaled variability should approach the surface flux and P_{scale} and F_{scale} should converge to 1. Smaller bandwidths, on the one hand, result in smaller scaling factors. The values listed in Table 1, for example, indicate that P_{scale} and F_{scale} for the 600–1800 bands are systematically lower than for the other bands. This is consistent with the idea that the contribution of long timescales (>10 min) to the total flux is relatively smaller than the contribution of shorter timescales (e.g., <10 min). On the other hand, a non-homogeneous surface distribution of VOC emissions will introduce more variability resulting in systematically higher scaling factors. The variability for all three sites is larger than expected. The sum of the $P_{60–600}$ ($F_{60–600}$) and $P_{600–1800}$ ($F_{600–1800}$) factors from Table 2, for example, is close or greater than 1 for all cases. Adding these two bands together, however, does not account for the contribution of eddies that transport the flux on timescales between 0.1 and 60 s. This range is expected to carry a substantial portion of the surface flux (see Fig. 3), typically ranging between 20% and 30%. We, therefore, conclude that the heterogeneity of surface emissions is evident at all three sites.

Analysis of the three dataset suggests that surface emissions of isoprene and methanol in Michigan seemed to be distributed more evenly than at the tropical rainforest in La Selva. Duke forest (a loblolly pine plantantion with sweetgum in the understory) was characterized by the highest scaling values, suggesting that this site was the least homogenous. The low variability observed at the Prophet site is somewhat surprising as it is surrounded by two big lakes approximately 1 km to the north and 2–3 km to the south. Vegetation maps show that the main isoprene emitting species in Michigan is Big tooth Aspen intercepted by patches of Maple trees, which do not emit isoprene. The La Selva site in particular is characterized by a high abundance of isoprene emitting species [32]. We attribute the larger variability observed at the tropical and the loblolly pine sites (on average, 70% higher surface layer scaling variables than observed at the Prophet tower) to the high species diversity in tropical ecosystems [33] and the patched heterogeneous landscape surrounding the pine plantation. The highest variability of surface emissions was measured for methanol at Duke forest. Arial photographs of this plantation (http://c-h2oecology.env.duke.edu/Duke-FACE/description.cfm) show that this site is surrounded by a patchwork of different landscapes. The plantation itself consists of loblolly pines, which do not emit isoprene, and sweet gum, a strong isoprene emitter, growing in the under story. Despite these differences the variability of isoprene is similar to that observed at the tropical site. Our analysis shows that at non-ideal locations, site specific proportionality constants can be derived that relate the observed variance to the surface flux.

3. Conclusion

Analysis of recent flux data sets collected using the PTR-MS instrument suggest that the variance method could be an alternative for estimating surface layer VOC fluxes under conditions with reasonably high VOC fluxes

(>0.2 mg m^{-2} h^{-1}). A better sensitivity could be achieved by using higher sampling rates (e.g., <5 s). The proportionality constants (P_{scale} and F_{scale}) that relate the variance over a certain time period to the surface flux were influenced by two counteracting processes: (1) undersampling of the turbulent flux causing lower scaling constants and (2) surface heterogeneity of VOC emissions resulting in higher variances and higher scaling constants. Once appropriate scaling factors from fast VOC measurements (e.g., the PTR-MS) are established, the variance relationships should theoretically be applicable independent from the measurement site. On average (using data from all three sites), we derive mixed layer scaling variables (P_{scale}) for isoprene on the order of 0.9 ± 0.4, 1.1 ± 0.4 and 0.7 ± 0.2 for the three most robust bands $P_{S60–300}$, $P_{S60–600}$ and $P_{S600–1800}$, respectively. The surface layer scaling variables (F_{scale}) are of comparable magnitude around 0.9 ± 0.3, 1.0 ± 0.4 and 0.6 ± 0.1 for $F_{S60–300}$, $F_{S60–600}$ and $F_{S600–1800}$, respectively. Thus, on average, without knowledge of the individual scaling variables, the isoprene flux could be determined within an accuracy of ~35%, 40% and 28% using the above mean values. The variance method could become an attractive alternative for flux measurements in situations where exact collocation of the sonic anemometer and the sampling inlet is not possible (e.g., at sites without easy canopy access) or where fast wind data are not available at the same time as the chemical measurements. An example is the deployment of a PTR-MS system on aircraft, which do not provide 10 Hz wind data. On the other hand, the methanol variability seems to be significantly enhanced at Duke forest, most likely due to non-homogeneous emissions. However, more data are needed to be able to generalize the variance method for methanol. It appears that non-homogeneous surface emissions and mesoscale variability can offset the variance by a factor of 2–3. This variability in turn could provide a useful metric for assessing surface heterogeneity. Comparison with relatively homogeneous surface emissions (e.g., CO_2 fluxes) could reveal differences caused by non-evenly distributed VOC surface sources.

The variability–lifetime analysis suggested that concentration changes attributed to mesoscale processes become more significant on time scales above 10 min for methanol and acetone; for timescales greater than 2 h the variances (σ_C/C) in the SL for these compounds are mainly governed by large scale airflow and appear to be proportional to the concentration jump between the PBL and the FT (according to Eq. (9). Fig. 2a and b depicts how the variability (σ_C/C) dependence increases on longer timescales, falling close to the prediction of the 1D vertical diffusion model. Assuming tropospheric lifetimes of VOCs are known, the variability–lifetime relationship can be used for estimating surface fluxes of biogenic VOCs over extended forested areas based on measurements of mean scalar concentrations in the PBL.

We conclude that the PTR-MS technique is a useful tool for assessing the variability of VOCs on different timescales allowing observations of processes occurring on small periods (<30 min) typically related to surface emissions, as well as larger periods (>1 h), caused by mesoscale variations. Taking advantage of the fast monitoring capabilities of the PTR-MS system, variability measurements of biogenic VOCs could be used for assessing the magnitude and homogeneity of surface fluxes and characterizing atmospheric lifetimes in remote places.

Acknowledgements

The National Center for Atmospheric Research is sponsored by The National Science Foundation. We thank Don Lenschow, David Gurarie and Ian Faloona for fruitful discussions and Mark Potosnak, Deborah Clark and Mary-Ann Carroll for technical and logistical support. This work was also in part supported by an Interagency Agreement (DW49939559) with the National Risk Management Research Laboratory of the U.S. Environmental Protection Agency and by NSF grant ATM-0119995.

References

[1] C.E. Junge, Tellus 26 (1974) 477.
[2] A.D. Gibbs, W.G.N. Slinn, J. Geophys. Res. 78 (1973) 574.
[3] D.H. Ehhalt, F. Rohrer, A. Wahner, M.J. Prather, D.R. Blake, J. Geophys. Res. 103 (1998) 18981.
[4] B.T. Jobson, S.A. McKeen, D.D. Parrish, F.C. Fehsenfeld, D.R. Blake, A.H. Goldstein, S.M. Schauffler, J.W. Elkins, J. Geophys. Res. 104 (1999) 16090.
[5] D.H. Lenschow, D. Gurarie, J. Geophys. Res. 107 (2002) (doi: 10.1029/2002JD002526).
[6] R. Jaenicke, in: H.W. Georgi, W. Jaschke, D. Reidel (Eds.), Chemistry of the Polluted and Unpolluted Troposphere, Norwell, MA, 1982, p. 341.
[7] J.C. Wyngaard, R.A. Brost, J. Atmos. Sci. 41 (1984) 102.
[8] E.G. Patton, P.P. Sullivan, K.J. Davis, Q. J. R. Meteorol. Soc. 129 (2003) 1415.
[9] B.T. Jobson, D.D. Parrish, P. Goldan, W. Kuster, F.C. Fehsenfeld, D.R. Blake, N.J. Blake, H. Niki, J. Geophys. Res. 103 (1998) 13557.
[10] J. Williams, H. Fischer, G.W. Harris, P.J. Crutzen, P. Hoor, A. Hansel, R. Holzinger, C. Warneke, W. Lindinger, B. Scheeren, J. Lelieveld, J. Geophys. Res. 105 (2000) 20473.
[11] T. Karl, P.J. Crutzen, M. Mandl, M. Staudinger, A. Guenther, A. Jordan, R. Fall, W. Lindinger, Atmos. Environ. 35 (2001) 5287.
[12] C. Warneke, J.A. de Gouw, Atmos. Environ. 35 (2001) 5923.
[13] HJ.I. Rinne, A.B. Guenther, C. Warneke, J.A. de Gouw, S.L. Luxembourg, J. Geophys. Res. 28 (2001) 3139.
[14] T. Karl, A. Guenther, C. Lindinger, A. Jordan, R. Fall, W. Lindinger, J. Geophys. Res. 106 (2001) 24157.
[15] T. Karl, C. Spirig, J. Rinne, C. Stroud, P. Prevost, J. Greenberg, R. Fall, A. Guenther, Atmos. Chem. Phys. 2 (2002) 279.
[16] W. Lindinger, A. Hansel, A. Jordan, IJMS 173 (1998) 191.
[17] A. Hansel, A. Jordan, C. Warneke, R. Hozinger, A. Wisthaler, W. Lindinger, Plasma Sources Sci. Technol. 8 (1999) 332.
[18] J.A. de Gouw, C. Warneke, T. Karl, G. Eerdekens, C. van der Veen, R. Fall, Int. J. Mass Spectrom. 223 (2003) 365.
[19] C. Torrence, G.P. Compo, Bull. Am. Meteorol. Soc. 79 (1997) 61 http://www.mathworks.com/products/wavelet/technicalliterature.jsp.

[20] D. Riemer, T. Thornberry, M.A. Carroll, S. Sillmann, G.J. Keeler, J. Sagady, D. Hooper, K. Paterson, J. Geophys. Res. 106 (2001) 24315.
[21] S. Madronich, J.G. Clavert, NCAR Technical Note 333 + STR, National Center for Atmospheric Research, Boulder, CO, 1989.
[22] I. Faloona, D. Tan, W. Brune, J. Hurst, D. Barket, T.L. Couch, P. Shepson, E. Apel, D.D.H. Lenschow, I.R. Paluch, A.R. Bandy, D.C. Thornton, D.R. Blake, I. Simpson, J. Geophys. Res. 104 (1999) 16275.
[23] J.C. Weil, J. Atmos. Sci. 47 (1990) 501.
[24] A. Guenther, C.N. Hewitt, D. Erickson, R. Fall, C. Geron, T. Graedel, P. Harley, L. Klinger, M. Lerdau, W.A. McKay, T. Pierce, B. Scholes, R. Steinbrecher, R. Tallamraju, J. Taylor, P. Zimmerman, J. Geophys. Res. 100 (1995) 8873.
[25] Q. Wang, D.H. Lenschow, L.L. Pan, R.D. Schillawski, G.L. Kok, A.S.H. Prevot, K. Laursen, L.M. Russell, A.R. Bandy, D.C. Thornton, K. Suhre, J. Geophys. Res. 104 (1999) 21767.
[26] D. Lenschow, I.R. paluch, A.R. Bandy, D.C. Thornton, D.R. Blake, I. Simpson, J. Geophys. Res. 104 (1999) 16275.
[27] S. Kimmel, J. Wyngaard, M. Otte, J. Atmos. Sci. 59 (2002) 1124.
[28] J.J. Finnigan, R.H. Shaw, Boundary-Layer Meteorol. 96 (2000) 211.
[29] D.K. Lilly, Q.J. Roy, Meteorol. Soc. 94 (1968) 292.
[30] M.L. Wesely, Boundary-Layer Meteorol. 44 (1988) 13.
[31] R. Stull, An Introduction to Boundary Layer Meteorology, Kluwer Academic Publishers, 1999.
[32] C. Geron, A. Guenther, J. Greenberg, H.W. Loescher, D. Clark, B. Baker, Atmos. Environ. 36 (2002) 3793.
[33] P. Harley, P. Vasconcellos, L. Vierling, C.C. Pinheiros, J. Greenberg, A. Guemther, L. Klinger, S.S.D. Almeida, D. Neill, T. Baker, O. Phillips, Y. Malhi, Global Change Biol. 10 (2004) (doi: 10.1111/j.1529-8817.2003.00760.x).